JOURNAL OF COMPUTATIONAL PHYSICS 117, 171–178 (1995)

An Optimized Method for Treating Long-Range Potentials

VINCENT NATOLI

Corporate Research Science Laboratories, Exxon Research and Engineering Company, Annandale, New Jersey 08801

AND

DAVID M. CEPERLEY

The National Center for Supercomputing Applications, Urbana, Illinois 61821

Received November 30, 1992; revised October 28, 1994

In simulations of systems with periodic boundary conditions, the Ewald image method is used to evaluate long-range potentials by constructing infinite but rapidly converging sums in both real space and reciprocal space. However, the traditional Ewald construction is not optimal for the case where the real and reciprocal space sums are truncated. We derive a criterion which is used to determine the accuracy of a given approximation and use this criterion to determine the optimal separation of a very general class of potentials, subject to cutoffs, k_c and r_c, in reciprocal and real space, respectively. Using a basis of locally piecewise-quintic Hermite interpolants, we demonstrate our procedure and show that for the Coulomb potential, the error is proportional to $\exp(-k_c r_c)$. At typical cutoff values we find the optimized breakup to be two orders of magnitude more accurate than the standard Ewald breakup for a given computational effort. © 1995 Academic Press, Inc.

I. INTRODUCTION

In simulation methods such as classical Monte Carlo (MC), molecular dynamics (MD), and quantum Monte Carlo (QMC), the presence of long-range potentials and pair wavefunctions requires the careful use of the method of images in periodic boundary conditions (PBC). The potential or pair wavefunction due to a given particle and all its images converges slowly in real space, but it is possible to divide the sum into parts in real space and reciprocal space, each of which converges rapidly [1, 2].

It is important for several reasons that the periodic image potential be accurately computed. First, it enables one to easily specify the conditions of the simulation, allowing comparisons between different computer codes. Second, the image potential yields results closer to the thermodynamic limit. For example, since the random phase approximation is exact at long wavelengths, accurate Fourier components of the potential must be used to guarantee the correct long wavelength properties of a charged system. Finally, it is easier to perform model calculations, such as Hartree–Fock on a simulation cell with the exact image potential and then to use those results to extrapolate to the bulk limit.

We assume that the interaction between two particles is given by a spherically symmetric potential $V(|\mathbf{r}|)$, where $|\mathbf{r}|$ is the radial distance between the two particles. We further assume that V can be split into a short-range piece which vanishes for r greater than r_c and a part that is Fourier transformable. The image potential is defined by summing over the interaction between a particle and the replicas of the other particle in periodic space,

$$V_p(\mathbf{r}) = \sum_{\mathbf{l}} V(|\mathbf{r} + \mathbf{l}|). \tag{1}$$

Here $\mathbf{l}$ are the Bravais lattice vectors of the simulation box, i.e., $(n_x L_x, n_y L_y, n_z L_z)$, where n_x, n_y, n_z are integers and L_x, L_y, L_z are the dimensions of the box. Applying the Poisson sum formula [3] we have

$$V_p(\mathbf{r}) = \sum_{\mathbf{k}} V_k e^{i\mathbf{k}\cdot\mathbf{r}}, \tag{2}$$

where $\mathbf{k}$ are the reciprocal lattice vectors of the periodic box, $\mathbf{k} = 2\pi(n_x/L_x, n_y/L_y, n_z/L_z)$, and

$$V_k = \frac{1}{\Omega}\int_\Omega d^3\mathbf{r} e^{-i\mathbf{k}\cdot\mathbf{r}} V_p(\mathbf{r}). \tag{3}$$

The volume of the simulation box is $\Omega = L_x L_y L_z$.

The effect of PBC is that the "bare" potential is used on a discrete lattice in k-space, i.e., only those $\mathbf{k}$ vectors that are reciprocal lattice vectors of the simulation box. As the size of the system increases, that set becomes more dense. In the limit of an infinitely large box that set is continuous.

Both the real space and k-space forms of this potential, $V_p(r)$, involve infinite sums and are not convenient for computation since they may be very slowly convergent. But if the sum is

0021-9991/95 $6.00
Copyright © 1995 by Academic Press, Inc.
All rights of reproduction in any form reserved.

broken into a part in real space *and* a part in k-space, both sums can converge exponentially fast. In the case of the Coulomb potential, where $V(r) = 1/r$ and $V_k = 4\pi/\Omega k^2$, the standard breakup [1] which uses a Gaussian charge distribution gives

$$V_p(\mathbf{r}) = \frac{4\pi}{\Omega}\sum_{\mathbf{k}} e^{i\mathbf{k}\cdot\mathbf{r}}\frac{e^{-k^2/4G^2}}{k^2} + \sum_{\mathbf{l}}\frac{1}{|\mathbf{l}-\mathbf{r}|}\operatorname{erfc}\{G|\mathbf{l}-\mathbf{r}|\}, \quad (4)$$

where G is a parameter chosen to optimize the convergence properties in k-space and real space.

In this paper we show how to optimally construct this breakup, independent of the actual potential, V, and subject to real and reciprocal space cutoffs. Thus we generalize and optimize methods used by Ewald for the Coulomb interaction. Preserving the general form of the Ewald separation, we approximate the image potential by a sum in k-space and a sum in real space,

$$V_a(\mathbf{r}) = \sum_{\mathbf{l}} W(|\mathbf{r}+\mathbf{l}|) + \sum_{|\mathbf{k}|\le k_c} Y_k e^{-i\mathbf{k}\cdot\mathbf{r}}, \quad (5)$$

where $V_a(r)$ is an approximation to $V_p(r)$ because k_c is finite. $W(r)$ is chosen to vanish smoothly as $|\mathbf{r}|$ approaches r_c, where r_c is less than half of the distance across the simulation box in any direction. This constraint makes $W(r)$ a function of the minimum distance of a particle to any image, prevents overlap of the real space contribution between images, and avoids the sum over all lattice vectors. If either r_c or k_c goes to infinity, of course $V_a \to V_p$.

So far we have only discussed calculations on long-range potentials, which are all that is needed in classical mechanics. In quantum simulations, the image method must be used to represent long-range pair wavefunctions as well. For example, in using variational or diffusion Monte Carlo, the trial wavefunction must be periodic and differentiable throughout the simulation cell. A pair product trial wave function includes the factor

$$\Psi(\{R_i\}) = \exp\left(-\sum_{i<j} u(|r_i - r_j|)\right). \quad (6)$$

The arguments presented above for classical long-range potentials, apply directly to the pair function $u(r)$ if it is long-range. For charged particles, one difference from the classical situation is that the pair functions are analytically simple in k-space and not in real space. They are typically not a single inverse power law. For example, the RPA pair wavefunction for the electron gas has the form [4]

$$u_k = \frac{1}{2N}(-1 + \sqrt{1 + 12r_s/k^4}). \quad (7)$$

Since the method described here requires only the Fourier representation of the periodic function, this presents no additional complications.

To summarize, we derive a criterion to measure the accuracy of an approximate potential used in the simulation of a system of N particles. Given this accuracy measure, we derive and evaluate an algorithm which has been used extensively by one of us (DMC), but not previously published. This algorithm determines the optimal breakup of the exact potential into sums in real and reciprocal space subject to truncation at r_c and k_c. Section 2 discusses a completely general, basis-independent, derivation of the optimal breakup. Section 3 chooses a basis of locally piecewise-quintic Hermite interpolants (LPQHI) to demonstrate the procedure. Section 4 presents results using the LPQHI basis on the Coulomb potential and Section 5 outlines our conclusions.

II. OPTIMIZATION OF THE BREAKUP

It is shown in the Appendix that to minimize error in the potential, it is appropriate to minimize the mean squared difference, χ^2, between $V_p(\mathbf{r})$ and its approximation $V_a(\mathbf{r})$,

$$\chi^2 = \frac{1}{\Omega}\int_\Omega d\mathbf{r}\left(V_p(\mathbf{r}) - W(r) - \sum_{|\mathbf{k}|\le k_c} Y_k e^{-i\mathbf{k}\cdot\mathbf{r}}\right)^2. \quad (8)$$

To optimize with respect to Y_k and $W(r)$, expand $W(r)$ in an arbitrary basis of J radial functions $h_n(r)$,

$$W(r) = \sum_{n=1}^{J} t_n h_n(r), \quad (9)$$

with unknown coefficients t_n. The set of Y_k which minimizes χ^2 is

$$Y_k = V_k - \sum_{n=1}^{J} c_{nk} t_n, \quad (10)$$

where

$$c_{nk} = \frac{1}{\Omega}\int_0^{r_c} d^3\mathbf{r} e^{-i\mathbf{k}\cdot\mathbf{r}} h_n(r) \quad (11)$$

and V_k are the Fourier components of $V_p(r)$ from Eq. (3). Note also that $V_k = V_{-k}$ and $Y_k = Y_{-k}$. Using Eq. (2), Eq. (9), and Eq. (10), we may reduce Eq. (8) to

$$\chi^2 = \frac{1}{\Omega}\int_\Omega d\mathbf{r}\left(\sum_{|\mathbf{k}|>k_c} V_k e^{i\mathbf{k}\cdot\mathbf{r}} - \sum_{n=1}^{J} t_n h_n(r) + \sum_{|\mathbf{k}|\le k_c}\sum_{n=1}^{J} c_{nk} t_n e^{i\mathbf{k}\cdot\mathbf{r}}\right)^2 \quad (12)$$

$$= \frac{1}{\Omega}\int_\Omega d\mathbf{r}\left(\sum_{|\mathbf{k}|>k_c} V_k e^{i\mathbf{k}\cdot\mathbf{r}} - \sum_{|\mathbf{k}|>k_c}\sum_{n=1}^{J} c_{nk} t_n e^{i\mathbf{k}\cdot\mathbf{r}}\right)^2 \quad (13)$$

$$= \frac{1}{\Omega}\int_\Omega d\mathbf{r}\left(\sum_{|k|>k_c} e^{i\mathbf{k}\cdot\mathbf{r}}\left(V_k - \sum_{n=1}^{J} c_{nk}t_n\right)\right)^2. \tag{14}$$

Now expand out the squared term to get

$$\chi^2 = \frac{1}{\Omega}\int_\Omega d\mathbf{r}\left(\sum_{|k|>k_c}\sum_{|k'|>k_c} e^{i\mathbf{k}\cdot\mathbf{r}}e^{-i\mathbf{k}'\cdot\mathbf{r}} \left(V_k - \sum_{n=1}^{J} c_{nk}t_n\right)\left(V_{k'} - \sum_{n'=1}^{J} c_{n'k'}t_{n'}\right)\right). \tag{15}$$

Taking the derivative with respect to $t_{n'}$, we have

$$\frac{\partial\chi^2}{\partial t_{n'}} = \frac{2}{\Omega}\int_\Omega d\mathbf{r}\left(\sum_{|k|>k_c}\sum_{|k'|>k_c} e^{i\mathbf{k}\cdot\mathbf{r}}e^{-i\mathbf{k}'\cdot\mathbf{r}} \left(V_k - \sum_{n=1}^{J} c_{nk}t_n\right)c_{n'k'}\right). \tag{16}$$

Doing the integral on $\mathbf{r}$ results in a delta function and cancels the factor of Ω:

$$\frac{\partial\chi^2}{\partial t_{n'}} = 2\left(\sum_{|k|>k_c}\sum_{|k'|>k_c}\delta_{kk'}\left(V_k + \sum_{n=1}^{J} c_{nk}t_n\right)c_{n'k'}\right) \tag{17}$$

$$= 2\left(\sum_{|k|>k_c}\left(V_k + \sum_{n=1}^{J} c_{nk}t_n\right)c_{n'k'}\right). \tag{18}$$

Finally, setting this derivative to zero we have a set of linear equations,

$$\sum_{n=1}^{J}\sum_{|k|>k_c} c_{lk}c_{nk}t_n = \sum_{|k|>k_c} V_k c_{lk}. \tag{19}$$

To summarize, the procedure to find the optimal breakup is first to calculate V_k and the c_{nk} as defined in Eq. (11). Then the linear set of Eqs. (19) is solved for t_n. The singular value decomposition (SVD) [5] method is used to solve the equations for t_n, because the matrices are ill-conditioned. Finally, from Eq. (15) it is easy to show that

$$\chi^2 = \sum_{|k|>k_c} Y_k^2. \tag{20}$$

There are several parameters which will determine how closely V_a approximates V_p. The real space cutoff, r_c, is usually taken to be one-half the shortest length across the simulation cell, so at most one image will contribute to the sum. The k-space cutoff, k_c, determines the number of k vectors used in the sum and the accuracy of the approximation. In Eq. (19), the sums are taken over the values of k for $|\mathbf{k}| > k_c$. In practice we sum for $k_c < |\mathbf{k}| \le K$. If K is chosen too small, the procedure can become unstable. K and the number of basis functions, J, are increased until it is clear that χ^2 is converged.

Minimizing χ^2 will get the best breakup for the potential but not necessarily for its derivatives. These are needed in quantum Monte Carlo because the second derivative of the pair function is used in the expression for kinetic energy. Wild variations of the second derivative near the endpoints would introduce error into the kinetic energy calculation. Likewise, in classical simulations it is often desirable to minimize error in the forces which are proportional to the first derivative of V. These cases result in minor modifications to Eqs. (19). For example, we find that to minimize the error in the first derivative Eq. (19) is replaced by

$$\sum_{n=1}^{J}\sum_{|k|>k_c} k^2 c_{lk}c_{nk}t_n = \sum_{|k|>k_c} k^2 V_k c_{lk}. \tag{21}$$

This can be seen by writing a new expression for χ^2 which minimizes the error in the forces,

$$\chi^2 = \frac{1}{\Omega}\int_\Omega d\mathbf{r}\left(\nabla V_p(\mathbf{r}) - \nabla W(r) + \sum_{|k|\le k_c} i\mathbf{k}Y_k e^{-i\mathbf{k}\cdot\mathbf{r}}\right)^2. \tag{22}$$

Again taking the derivative with respect to Y_k and substituting back in Eq. (22) with Eq. (9) and Eq. (3) we find

$$\chi^2 = \frac{1}{\Omega}\int_\Omega d\mathbf{r}\left(\sum_{|k|>k_c} -i\mathbf{k}V_k e^{i\mathbf{k}\cdot\mathbf{r}} - \sum_{|k|>k_c}\sum_{n=1}^{J} -i\mathbf{k}c_{nk}t_n e^{i\mathbf{k}\cdot\mathbf{r}}\right)^2. \tag{23}$$

Taking the derivative with respect to t_n as before we arrive at Eq. (21) with the final expression for χ^2 being

$$\chi^2 = \sum_{|k|>k_c} k^2 Y_k^2. \tag{24}$$

The results of this section are completely general and independent of the basis functions, $h_n(r)$, chosen to represent the short-range real space function $W(r)$. In the next section we describe the implementation of the method with a piecewise polynomial basis.

III. THE LPQHI BASIS

We now need to choose a basis to represent $W(r)$, keeping in mind that for a Coulomb potential this is an error function, a function which is rapidly decreasing at large r. To illustrate our method we have chosen to use fifth-order polynomials, defined on intervals (r_i, r_{i+1}), where r_i are the knot values. We use $m + 1$ equally spaced knots starting at 0 and ending at r_c. Hence $r_i = \Delta i$, $0 \le i \le m + 1$, and $\Delta = r_c/m$. This basis is known as a locally piecewise-quintic Hermite interpolant

(LPQHI). It should be emphasized that this choice of basis is not unique. The argument of Section 2 is independent of the basis chosen. The advantages of this basis are that it is applicable to rapidly varying functions, it is not seriously overcomplete, it is easily expandable through the addition of more knots, and it accommodates constraints at the endpoints. For example, to set the first derivative at the origin to the known cusp value, one simply removes this variable from the fit.

Our unknown variables are the values of $W(r)$ and its first and second derivatives at the knot values, which we denote $t_n = t_{i\alpha}$, where i is the knot value with $0 \le i \le m$ and α is the derivative $0 \le \alpha \le 2$. We include second derivatives because it is important to have smooth second derivatives in QMC. A fifth-order polynomial is then used to interpolate between the knots.

The basis functions corresponding to this choice of parameterization of $W(r)$ are piecewise-quintic interpolants that have a single derivative equal to unity and the other derivatives vanishing. Our basis functions are, therefore,

$$h_{i\alpha}(r) = \begin{cases} (\Delta)^\alpha \sum_{n=0}^{5} S_{\alpha n} \left(\frac{r - r_i}{\Delta}\right)^n, & r_i < r \le r_{i+1}, \\ (-\Delta)^\alpha \sum_{n=0}^{5} S_{\alpha n} \left(\frac{r_i - r}{\Delta}\right)^n, & r_{i-1} < r \le r_i, \\ 0, & \text{otherwise}, \end{cases} \tag{25}$$

where [6]

$$S_{\alpha n} = \begin{bmatrix} 1 & 0 & 0 & -10 & 15 & -6 \\ 0 & 1 & 0 & -6 & 8 & -3 \\ 0 & 0 & \frac{1}{2} & -\frac{3}{2} & \frac{3}{2} & -\frac{1}{2} \end{bmatrix}. \tag{26}$$

(Note the addition of a new index that describes the derivative of W.) Figure 1 shows half of the functions h_{i0}, h_{i1}, and h_{i2}, the other three functions being merely mirror images.

The required c_{nk} are here $c_{i\alpha k}$ and are calculated as

$$c_{i\alpha k} = \frac{1}{\Omega} \int_0^{r_c} d^3r\, e^{-i\mathbf{k}\cdot\mathbf{r}} h_{i\alpha}(r) \tag{27}$$

$$= \Delta^\alpha \sum_{n=0}^{5} S_{\alpha n} (D^+_{ikn} + D^-_{ikn}(-1)^{\alpha+n}), \tag{28}$$

where

$$D^\pm_{ikn} = \pm \frac{1}{\Omega} \int_{r_i}^{r_{i\pm1}} d^3r\, e^{-i\mathbf{k}\cdot\mathbf{r}} \left(\frac{r - r_i}{\Delta}\right)^n. \tag{29}$$

This integral can be calculated recursively as follows. If we define

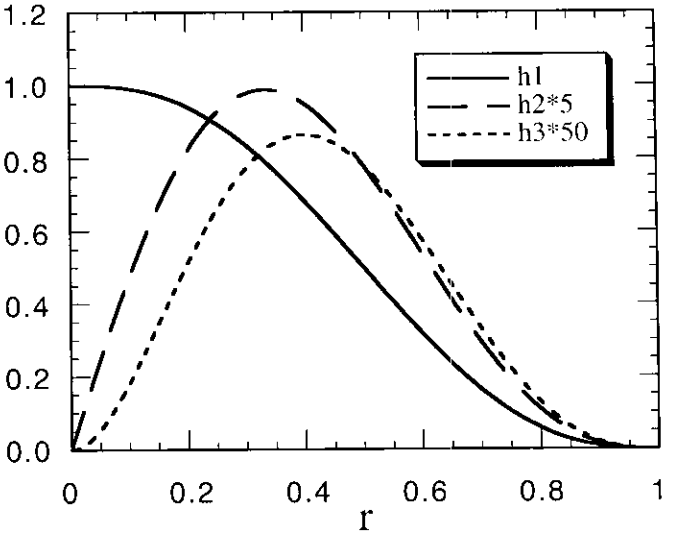

FIG. 1. The upper basis functions h_{i0}, h_{i1}, h_{i2} in an arbitrary interval i. The lower functions are obtained by reflecting $x \to -x$.

$$E^\pm_{ikn} = \pm \frac{4\pi}{\Omega k} \int_{r_i}^{r_{i\pm1}} dr\, e^{ikr} \left(\frac{r - r_i}{\Delta}\right)^n, \tag{30}$$

then

$$D^\pm_{ikn} = \Delta\, \mathrm{Im}\{E^\pm_{ik(n+1)} + i\, E^\pm_{ikn}\}. \tag{31}$$

For $n = 0$, $E^\pm_{ik0}$ can be evaluated and for $n > 0$; $E^\pm_{ikn}$ may be calculated by integrating by parts. For example,

$$E^\pm_{ik0} = \mp \frac{4\pi i}{\Omega k^2} (e^{\pm ik\Delta} - 1) e^{ikr_i}, \tag{32}$$

and for $n > 0$,

$$E^\pm_{ikn} = -\frac{i}{k} \left[\frac{4\pi}{\Omega k} (\pm 1)^{n+1} e^{ikr_{i\pm1}} - \frac{n}{\Delta} E^\pm_{ikn-1} \right]. \tag{33}$$

In the case of the Coulomb potential, there is a singularity at $r = 0$, which will also be present in $W(r)$. Since this would make tabulation of the function difficult and less accurate for small r, we find it beneficial to incorporate the singularity into the basis functions,

$$h_{i\alpha}(r) = \frac{1}{r} \sum_{n=0}^{5} S_{\alpha n} \left(\frac{r - r_i}{\Delta}\right)^n, \tag{34}$$

so that the new equation for $D^\pm_{ikn}$ is

$$D^\pm_{ikn} = \mathrm{Im}\{E^\pm_{ikn}\}. \tag{35}$$

Using the $D^{\pm}_{ikn}$ from Eq. (35) in the expression for c_{iak} in Eq. (28), we are in a position to solve the set of linear equations Eq. (19) for t_n. The t_n are then used to construct $W(r)$ and the Fourier sum.

IV. RESULTS FOR THE COULOMB POTENTIAL

To evaluate the behavior of the optimized fit using the LPQHI basis, χ^2 was calculated for various values of r_c and k_c for the Coulomb potential. We used $m = 40$ knots and KL was approximately 3000, where L is the size of the cubic simulation cell. These values for m and K resulted in good convergence in χ^2. We find that the rms error in the fit is well described by the equation

$$\chi \approx 0.77 \frac{e^2}{L} e^{-k_c r_c}. \tag{36}$$

We also computed χ^2 for the usual Ewald breakup, subject to the same real space and k-space cutoffs,

$$V_{\mathrm{Ew}}(\mathbf{r}) = e^2 \left\{ \sum_{\mathbf{l}} \frac{1}{|\mathbf{l}-\mathbf{r}|} \operatorname{erfc}(G|\mathbf{l}-\mathbf{r}|)\Theta(r_c - |\mathbf{r}|) + \frac{4\pi}{\Omega} \sum_{|\mathbf{k}|<k_c} \frac{e^{-k^2/4G^2}}{k^2} e^{i\mathbf{k}\cdot\mathbf{r}} \right\}. \tag{37}$$

Note that the function θ is defined as 1 when its argument is positive, and 0 otherwise. An expression for χ^2 can be derived just as before. If this is put entirely into k-space and the integration over $\mathbf{r}$ is done we get

$$\chi^2 = \sum_{k} \Delta_k^2, \tag{38}$$

where

$$\Delta_k = \frac{4\pi e^2}{\Omega} \left[\frac{1}{k^2} - \frac{1}{k} \int_0^{r_c} dr \sin(kr) \operatorname{erfc}(Gr) - \frac{e^{-k^2/4G^2}}{k^2} \Theta(|\mathbf{k}| - k_c) \right]. \tag{39}$$

The value of G which minimizes χ^2 is found to be approximately $\sqrt{k_c/2r_c}$. Note that the sum, Eq. (38), is over all points in k-space, not just $|\mathbf{k}| > k_c$, because the real space function is cut off at r_c. This sum may be transformed into an integral over k-space and then done numerically. Figure 2 shows $\mathrm{Ln}[\chi/(e^2/L)]$ versus $k_c r_c$, for the optimized fit and the truncated Ewald case. For values of k_c and r_c of practical interest, our procedure gave up to a factor of 100 improvement in accuracy over the usual breakup. Figure 3 gives the same plot, but for χ^2 which minimizes forces as described by Eq. (22). It shows $\mathrm{Ln}[\chi/(e^4/L^2)]$ versus $k_c r_c$. This also demonstrates the superiority of the optimized breakup when minimizing the error in forces. We find that codes using optimized breakups run twice as fast (for the same accuracy) as the standard breakup. Figure 4 compares the charge associated with the potential $W(r)$ from the optimized fit with the Ewald case, using Poisson's equation

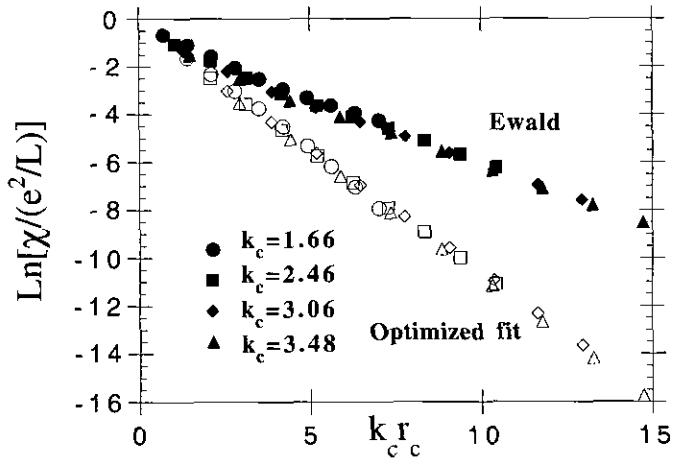

FIG. 2. $\mathrm{Ln}[\chi/(e^2/L)]$ versus the dimensionless parameter $k_c r_c$ for various values of k_c. The open symbols represent results for the optimized fit and the filled symbols represent results for the cutoff Ewald case.

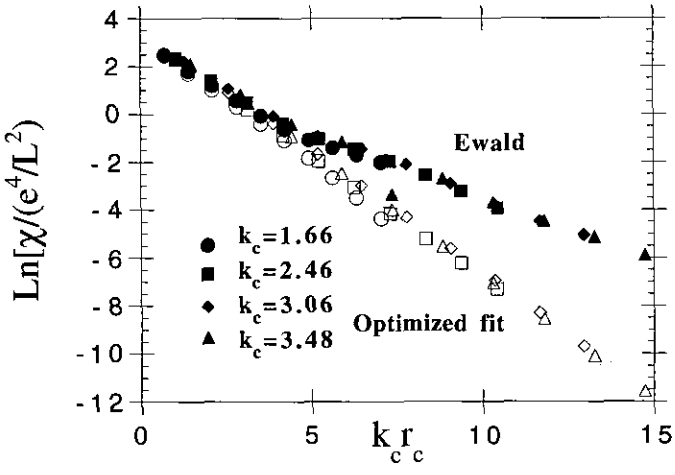

FIG. 3. $\mathrm{Ln}[\chi/e^4/L^2)]$ versus the dimensionless parameter $k_c r_c$ for various values of k_c. This is the χ defined by Eq. (22) which minimizes the error in the forces. The open symbols represent results for the optimized fit and the filled symbols represent results for the cutoff Ewald case.

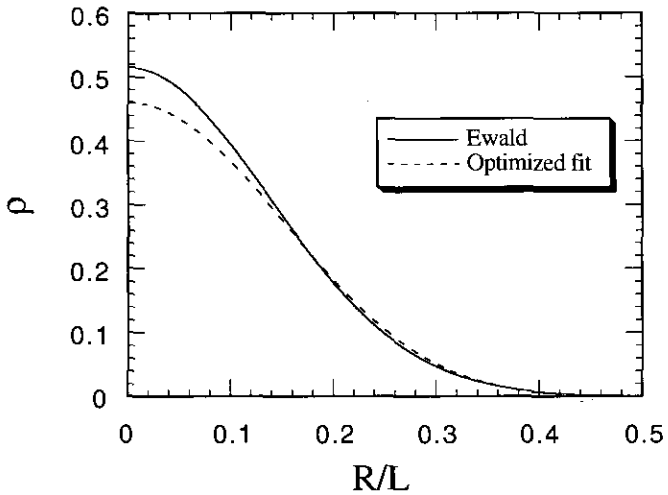

FIG. 4. Charge density ρ associated with the short range potential $W(r)$ versus r/L, for both the optimized fit and the cutoff Ewald case, where $k_c r_c = 13.3$.

$$\nabla^2 W(r) = 4\pi\rho. \tag{40}$$

The optimized density is more spread out but still decays to zero at the edge of the box, while a Gaussian is constrained to be more peaked to ensure that it is small enough at the edge. The optimization takes full advantage of the increased flexibility. Figure 5 compares $\mathrm{Ln}[Y_k]$ for these two cases and shows that the Fourier components of the optimized fit decay faster than those for the truncated Ewald.

While χ is a measure of the total error in the unit simulation cell, it does not indicate where in the unit cell that error is largest. Figure 6 is a plot of the integrand of Eq. (15) in a plane which slices through the center of the simulation cell. The numbers give a relative sense of where error is the largest.

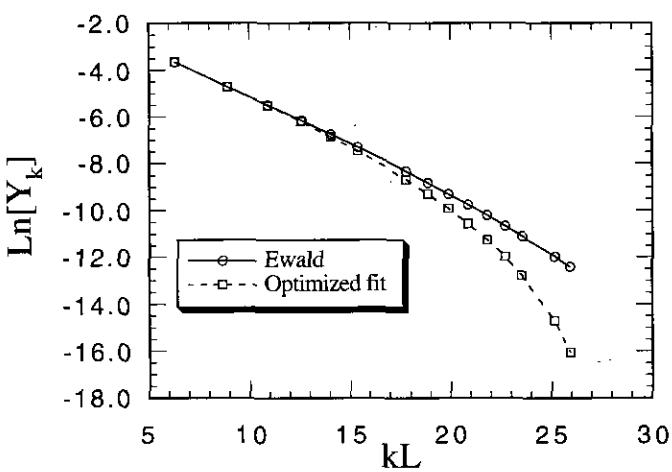

FIG. 5. $\mathrm{Ln}[Y_k]$ versus kL, for both the optimized fit and the cutoff Ewald case, where $k_c r_c = 13.3$.

It is of interest to find how computation time for a simulation step scales with the number of particles, N, for the Coulomb potential. The time for the real space sum will be proportional to Nr_c^3 because for N particles we must consider all the particles in a sphere with radius r_c. The time for the k-space sum will be proportional to $N^2k_c^3$ because again there are N particles and the number of k-vectors to sum over is proportional to k_c^3 multiplied by the density in k-space, which is proportional to the unit cell volume and consequently to N. In this case computation time is equal to $a_1 Nr_c^3 + a_2 N^2 k_c^3$ with a_1 and a_2 dependent on programming details. Using Eq. (36) for k_c in terms of χ and r_c and optimizing time with respect to r_c, we find that

$$\text{CPU time} \propto (N \,\mathrm{Log}[N])^{3/2}. \tag{41}$$

It is worth noting that in evaluating this expression, we have used the criterion defined by Eq. (46), which demonstrates that, for equivalent accuracy, χ should scale as $N^{-1/2}$. Ignoring this, we would get $T \propto N^{3/2}$, which is the usual expression given for the Ewald method.

V. CONCLUSIONS

We have presented a general method for optimizing the representation of long-range functions in simulations. As in the traditional Ewald method, the function is separated into finite reciprocal and real space sums. The procedure takes as input the Fourier components of the infinite system potential and computes a short-range real space function and the Fourier coefficients for the sum on k vectors. Our procedure yields the optimal breakup of the potential into sums of this form.

We find improved performance over the standard method. Additionally we find that the rms error, χ, is proportional to $\exp(-k_c r_c)$ and that the computation time scales as $(N \,\mathrm{Log}[N])^{3/2}$ for calculations of equivalent accuracy. The method described here is useful for classical and quantum systems, with long-range potentials and wavefunctions. The procedure is purely numerical and can be totally automated. It does not require any special properties of the potential. This is particularly useful when the potential or wavefunction is not a pure power law. If the potential contains a part at small r which is not Fourier transformable then that part can be removed and put directly into $W(r)$.

Other methods exist for the calculation of long-range forces and potentials. The traditional Ewald method is specific to the Coulomb potential and has been shown above to be unoptimized in cases where there are cutoffs in real and reciprocal space. There is also a class of order(N) algorithms developed by Greengard [7]. The Greengard method becomes more efficient [8] than traditional methods in periodic boundary conditions in three dimensions for N $\approx$ 1000–8000, depending on the desired precision. Simulations are often done with significantly

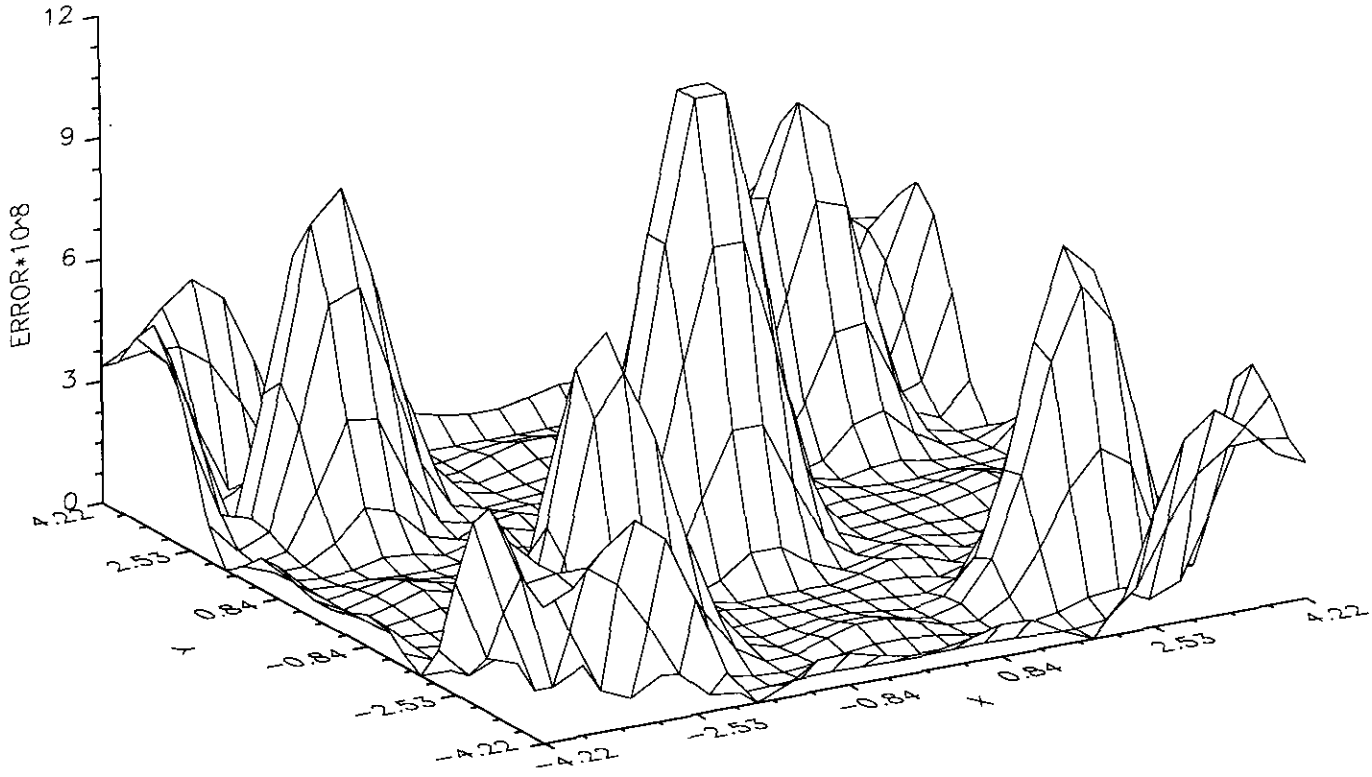

FIG. 6. The error between the optimized potential V_a and the true potential V_p plotted in a plane which passes through the center of the simulation cell. The function plotted is the integrand of Eq. (15).

fewer particles. In addition, the Greengard method, with its multipole expansion formalism, has not yet been extended to arbitrary potentials and only achieves a speedup when the total potential energy is being computed, e.g., in MD. For MC methods, where particles are moved one at a time, order(N) algorithms are not known.

VI. APPENDIX: DERIVATION OF THE χ^2 MEASURE

Let us consider how accurate a representation of the potential or pair function is needed. Consider first classical Monte Carlo. To sample the correct distribution, the change in potential divided by $k_B T$ as one particle is moved must be computed and compared to the logarithm of a random number to decide whether the move will be accepted. Clearly the results will not be seriously affected if the accuracy in the energy difference is less than ε, where $\varepsilon \ll 1$.

Consider a trial move from $\mathbf{r}_j$ to $\mathbf{r}_j'$. The error in the potential of the particle at $\mathbf{r}_j$, due to the use of the approximation Eq. (5), can be written as a Fourier expansion in k-space,

$$\begin{aligned} e(\mathbf{r}_j) &= \sum_{i \neq j} (V_p(\mathbf{r}_j - \mathbf{r}_i) - V_a(\mathbf{r}_j - \mathbf{r}_i)) \\ &= \sum_{i \neq j}^{N} \sum_{\mathbf{k}} e^{i\mathbf{k}\cdot(\mathbf{r}_i - \mathbf{r}_j)} \tilde{Y}_k . \end{aligned} \tag{42}$$

We show below that $\tilde{Y}_k$ is the same Y_k defined in Eq. (5). The mean squared error in the difference in potential energy between $\mathbf{r}_j$ and $\mathbf{r}_j'$ which comes into the acceptance probability is

$$\begin{aligned} \langle (\Delta V)^2 \rangle &= \langle |e(\mathbf{r}_j) - e(\mathbf{r}_j')|^2 \rangle \\ &= \left\langle \left| \sum_{\mathbf{k}} \tilde{Y}_k (\rho_k - e^{i\mathbf{k}\cdot\mathbf{r}_j})(e^{-i\mathbf{k}\cdot\mathbf{r}_j} - e^{-i\mathbf{k}\cdot\mathbf{r}_j'}) \right|^2 \right\rangle, \end{aligned} \tag{43}$$

where the brackets indicate averages over the points $\mathbf{r}_j$ and $\mathbf{r}_j'$ and $\rho_k = \sum_i e^{i\mathbf{k}\cdot\mathbf{r}_i}$. Using the definition for the structure factor, $S_k = (1/N)\langle \rho_k \rho_{-k} \rangle$ it can be shown in the limit of large N that

$$\langle (\Delta V)^2 \rangle \approx 2N \sum_{\mathbf{k}} \tilde{Y}_k^2 S_k . \tag{44}$$

When the optimization procedure is performed as outlined in Section 2 the difference in the Fourier coefficients of V_a and V_p is zero for $|\mathbf{k}| \leq k_c$ and it is Y_k for $|\mathbf{k}| > k_c$. Also, for large k, $S_k \approx 1$. Hence,

$$\langle (\Delta V)^2 \rangle \approx 2N \sum_{|\mathbf{k}| > k_c} Y_k^2 = 2N\chi^2, \tag{45}$$

with χ^2 defined in Eq. (8). In classical Monte Carlo, let us assume that we need $\langle \Delta V^2 \rangle^{1/2} < \varepsilon k_B T$. This implies that

$$\chi < \frac{\varepsilon k_B T}{\sqrt{2N}}. \tag{46}$$

We have derived an expression to determine how good χ should be in a classical simulation and we have shown that to minimize error in the potential it is appropriate to minimize χ^2 as defined by Eq. (8).

The equivalent results for quantum systems will be obtained by replacing $k_B T$ with 1. If there are inaccuracies in the trial function, they will increase the variational energy. In variational Monte Carlo, the potential energy is only averaged over. It does not directly affect the random walk. Thus one only needs to make an unbiased estimate of the image potential. Nonetheless, accurate trial functions lead to low variances. It is inefficient if the variance of this estimate contributes to the total variance of the simulation. Similar remarks apply to Green's function Monte Carlo and diffusion Monte Carlo, but in these cases inaccuracies in the trial function only increase the variance of the computed ground state energy as long as they are sufficiently small. Therefore we feel that a reasonable criterion for the accuracy of the pair function in QMC is $\chi < \varepsilon/\sqrt{2N}$.

ACKNOWLEDGMENTS

This work was supported by National Science Foundation Grant DMR-91-17822, the Department of Physics, and the National Center for Supercomputing Applications. One of us (V.N.) acknowledges the support of the NDSEG Fellowship Program. We gratefully acknowledge useful discussions with Richard M. Martin. Additional information and copies of this algorithm may be obtained by electronic mail from vnatoli@erenj.com.

REFERENCES

1. M. Allen and D. Tildesley, *Computer Simulation of Liquids* (Oxford Science, Oxford, 1990).
2. S. W. de Leeuw, J. W. Perram, and E. R. Smith, *Proc. R. Soc. London A* **373,** 27 (1980).
3. J. Ziman, *Principles of the Theory of Solids* (Cambridge Univ. Press, Cambridge, 1989), p. 319.
4. D. Ceperley, *Phys. Rev. B* **18,** 3126 (1978).
5. W. Press, S. Teukolsky, B. Flannery, and W. Vetterling, *Numerical Recipes* (Cambridge Univ. Press, Cambridge, 1988).
6. The matrix S_{an} may be derived from the matrix which relates the coefficients of an arbitrary polynomial to the value of the polynomial along with its first and second derivatives at the endpoints.
7. L. Greengard and V. Rokhlin, *J. Comput. Phys.* **73,** 325 (1987).
8. K. E. Schmidt and M. Lee, *J. Statist. Phys.* **63,** 1223 (1991).